

# 1 **A fast approximation for 1D Inversion of Transient** 2 **Electromagnetic Data by BP Neural Network and** 3 **improved Particle Swarm Optimization**

4 Ruiyou Li, Huaiqing Zhang\*, Nian Yu, Ruiheng Li, Qiong Zhuang

5 The State Key Laboratory of Transmission Equipment and System Safety and Electrical New  
6 Technology, Chongqing University, Chongqing, 400044, China

7 [1378546842@qq.com](mailto:1378546842@qq.com) (Ruiyou Li); [zhanghuaiqing@cqu.edu.cn](mailto:zhanghuaiqing@cqu.edu.cn) (Huaiqing Zhang); [61408155@qq.com](mailto:61408155@qq.com) (Nian Yu);  
8 [392361773@qq.com](mailto:392361773@qq.com) (Ruiheng Li) ; [779695034@qq.com](mailto:779695034@qq.com) (Qiong Zhuang)

9 \*Correspondence to: [zhanghuaiqing@cqu.edu.cn](mailto:zhanghuaiqing@cqu.edu.cn)

10 **Abstract.** As one of the most active nonlinear inversion methods in transient electromagnetic  
11 (TEM) inversion, the back propagation (BP) neural network has high efficiency because the  
12 complicated forward model calculation is unnecessary in iteration. The global optimization ability  
13 of the particle swarm optimization (PSO) is adopted for amending BP's sensitivity on initial  
14 parameters, which avoids it falling into local optimum. A chaotic oscillation inertia weight PSO  
15 (COPSO) is proposed in accelerating convergence. The COPSO-BP algorithm performance is  
16 validated by two typical testing functions, then by two geoelectric models inversion and a field  
17 example. The results show that the COPSO-BP method has better accuracy, stability and relative  
18 less training times. The proposed algorithm has a higher fitting degree for the data inversion, and  
19 it is feasible in geophysical inverse applications.

20 **Keywords:** transient electromagnetic inversion; BP neural network; particle swarm optimization;  
21 chaotic oscillation

## 22 **1 Introduction**

23 Transient electromagnetic (TEM) method applies the secondary receiving voltage induced by the  
24 rapid switching off pulse current, and then deduces the geoelectrical parameters consisting of the  
25 resistivities and thicknesses of the layers. The later is a typical TEM inversion issues with nonlinear  
26 feature. The linear inversion method was simple and widely used through linearization process,  
27 yet it is extremely dependent on initial parameters selection and resulting in poor inversion  
28 accuracy. Hence, the nonlinear inversion methods attract more geophysicists attention in recent  
29 years.

30 The artificial neural network(ANN) is one of the most active nonlinear inversion methods, it has

---

### **Conflicts of Interests**

The authors declare that they have no conflict of interest.

31 very high computation efficiency because the complicated forward model calculation is  
32 unnecessary in iteration. All the geoelectrical parameters and the forward model relations are  
33 implied in the weight and threshold parameters of ANN. And it is different from the non-linear  
34 Monte Carlo method with global space search solution (He et al., 2018; Jha et al., 2008; Pekşen et  
35 al., 2014; Sharma, 2012; Tran and Hiltunen, 2012). Srinivas et al. (2012) compared the inversion  
36 performance of BP, radial basis function(RBF) and generalized regression neural network (GRNN)  
37 in vertical electrical sounding data, then established a 1-D inversion model with BP and finally  
38 realized the parameters inversion. Maiti et al. (2012) proposed a Bayesian neural network training  
39 method in 1-D electrical sounding. Jiang et al. (2018) improved the training method for kernel  
40 principal component wavelet neural network and achieved the resistivity imaging. Jiang et al.  
41 (2016a) gave a learning algorithm based on information criterion (IC) and particle swarm  
42 optimization for RBF network which improves the global search ability. Johnson (2017) utilized  
43 neural network method to invert multi-layer georesistivity sounding. Jiang et al. (2016b) presented  
44 a pruning Bayesian neural network (PBNN) method for resistivity imaging and solved the  
45 instability, local minimization problems. Raj et al. (2014) solved non-linear apparent resistivity  
46 inversion problems with ANN. The ANN has been widely applied in electric prospecting data  
47 interpretation for its powerful fitting ability. However, the neural network method is sensitive to  
48 initial parameter settings and falls easily into local minimum. Lots improved methods were  
49 proposed for balancing the convergence rate and inversion quality. Zhang and Liu (2011) proposed  
50 ant colony optimization for ANN and applied in high density resistivity, acquired smaller  
51 inversion errors and higher determinant coefficients. Dai et al. (2014) suggested a differential  
52 evolution (DE) for BP which enhanced the global search ability. Marina et al. (2014) introduced  
53 the genetic algorithm for ANN.

54 The Particle swarm optimization (PSO) has simple structure, fast convergence rate, high  
55 accuracy and global optimization ability. Fernández et al. (2010) successfully introduced the PSO  
56 in 1-D resistivity inversion. Godio and Santilano (2018) applied it in geophysical inversion and  
57 deduced a depth resistivity earth model. Since the PSO's global searching performance, the BP's  
58 initial weights and thresholds can be trained by PSO and then the BP's global optimization ability  
59 can be improved. Comparing to the standard PSO (SPSO), a chaotic oscillation inertia weight PSO  
60 (COPSO) which can accelerate the convergence rate in the early stage was proposed naturally(Shi  
61 et al., 2009).

62 The paper structure is as following: the principle of PSO algorithm with different inertia  
63 weights schemes, the BP neural network and the proposed COPSO-BP algorithm are given in  
64 section 2. Then, the COPSO-BP algorithm performance is validated by two typical testing  
65 functions in section 3. And in later section, inversion simulations of a three-layer and five-layer

---

66 geoelectric models are carried out, the hidden layer neuron numbers determining method is put  
 67 forward and algorithms performance is compared.

## 68 **2 Principle of COPSO-BP Algorithms**

### 69 **2.1 Chaotic Oscillation PSO algorithm**

70 For  $N$ -dimensional optimization problem, supposing the position (resistivity and thickness for  
 71 layered model parameters inversion) and velocity(update speed) of the  $i$ -th particle (global search  
 72 group number) at time  $t$  are  $x_i = (x_{i1}, x_{i2}, \dots, x_{iN})$  and  $v_i = (v_{i1}, v_{i2}, \dots, v_{iN})$  respectively. Then, at time  
 73  $t+1$ , they can be calculated by the iterations as

$$74 \quad v_{id}^{t+1} = \omega \cdot v_{id}^t + c_1 r_1 (p_{id}^t - x_{id}^t) + c_2 r_2 (p_{gd}^t - x_{id}^t) \quad (1)$$

$$75 \quad x_{id}^{t+1} = x_{id}^t + v_{id}^{t+1} \quad (2)$$

76 where  $r_1, r_2$  are random value evenly distributed in the interval (0,1),  $c_1, c_2$  are learning factors  
 77 (usually equal to 2). And  $p_{id}, p_{gd}$  means the individual and global maximum.

78 The inertia weight parameter  $\omega$  affects the algorithm performance seriously. A fixed weight  
 79 always was used in the early time, and then various dynamic weights were proposed. Shi et al.  
 80 (2010) have summarized several methods as

$$81 \quad \omega_1(t) = \omega_s - (\omega_s - \omega_e) t / T_{\max} \quad (3)$$

$$82 \quad \omega_2(t) = \omega_s - (\omega_s - \omega_e) (t / T_{\max})^2 \quad (4)$$

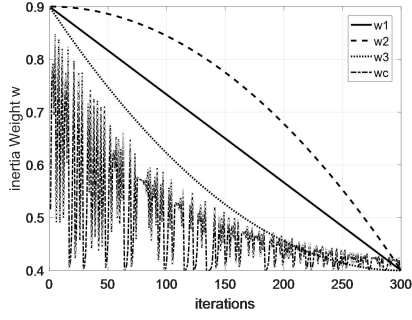
$$83 \quad \omega_3(t) = \omega_s - (\omega_s - \omega_e) \left[ 2t / T_{\max} - (t / T_{\max})^2 \right] \quad (5)$$

84 Where  $\omega_s$  and  $\omega_e$  are the start and end weight. The  $t, T_{\max}$  are the current and maximum iteration.  
 85 The above weights are of smooth and monotonically decreasing. In this paper, we proposed a  
 86 decreasing oscillation weights scheme which was based on chaotic logistic equation. Its specific  
 87 calculation formula as

$$88 \quad x_{t+1} = \mu x_t (1 - x_t) \quad t = 0, 1, 2, \dots, n \quad (6)$$

$$89 \quad \omega_e(t) = \omega_e + (\omega_s - \omega_e) (0.99^t \cdot x_t) \quad (7)$$

90 where  $\mu$  is the control parameter. A complete chaos state is established for  $x \in (0,1)$  and  $\mu = 4$ , an  
 91 inertia weight is then obtained from Eq.(7). Numerical experiments were carried out  
 92 correspondingly and showed that the initial value of  $x_0$  has little effect on inertia weight  $\omega$ . The  
 93 inertia weights comparison was shown in Fig.1 where  $x_0 = 0.234$  and  $\mu = 4$  for chaotic oscillation.

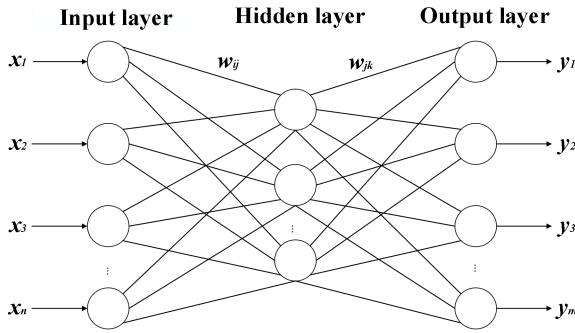


94

95 **Fig. 1** Inertial weight curves comparison

96 **2.2 BP Neural Network**

97 BP neural network is multi-layer feed forward structure, and a typical three-layer network is  
 98 shown in Fig. 2 (Yong et al., 2009).



99

100 **Fig. 2** Three-layer BP neural network structure

101 where  $x_1, x_2, \dots, x_n$  are the input value,  $y_1, y_2, \dots, y_m$  are the predicted output,  $w_{ij}, w_{jk}$  are the network  
 102 weights. The threshold parameter  $\alpha$  is defined in hidden layer with its output

103 
$$H_j = f\left(\sum_{i=1}^n w_{ij} x_i - \alpha_j\right) \quad j = 1, 2, \dots, l \quad (8)$$

104 where  $l$  is the hidden layer nodes numbers,  $f$  is the activation function with different expressions,  
 105 and the most widely used is sigmoid type function. The predicted output for the  $k$ -th unit is  
 106 calculated by

107 
$$O_k = \sum_{j=1}^l H_j w_{jk} - b_k \quad (9)$$

108 And parameter  $b$  means the output threshold. Then the prediction error can be determined based  
 109 on predicted output  $O_k$  and the expected output  $T_k$  as  $e_k = (T_k - O_k)O_k(1 - O_k)$ . The updating formula  
 110 for weights and thresholds are as following

$$\begin{cases}
w_{ij} = w_{ij} + \eta H_j (1 - H_j) x_i \sum_{k=1}^m w_{jk} e_k \\
w_{jk} = w_{jk} + \eta H_j e_k \\
\alpha_j = \alpha_j + \eta H_j (1 - H_j) \sum_{k=1}^m w_{jk} e_k \\
b_k = b_k + e_k
\end{cases} \quad (10)$$

112 where  $i=1,2,\dots,n; j=1,2,\dots,l; k=1,2,\dots,m$ ; and  $\eta$  is the learning rate.

### 113 2.3 BP Neural Network with COPSO algorithm

114 The initial parameters are chosen randomly, which affects the convergence rate, learning  
115 efficiency and perhaps falling into local minimum. The Chaotic Oscillation PSO (COPSO) has a  
116 much better global optimization capability, therefore, the COPSO algorithm is proposed to optimize  
117 the initial weight and threshold of BP. The COPSO-BP pseudo-codes were briefly described as  
118 following:

119

120 **Table.1** Pseudo-codes of COPSO-BP algorithm

- 
- 1: *BP network structure definition* (neuron numbers  $n, l, m$ , and *activation function*)
  - 2: *COPSO initialization for BP* (weights, threshold as  $X$ . PSO parameters as  $V_{\min}, V_{\max}, \omega, c_1, c_2$ , size  $M$ ,  $T_{\max}$ )
  - 3: *Initializing BP* with  $X_i$  ( $i=1, 2, \dots, M$ ) and *evaluating fitness* by Eq.(11) for each individual
  - 4: Setting the  $p_{id}$  and  $p_{gd}$
  - 5: **While**  $iter < T_{\max}$  **do**
  - 6:     updating inertia weight by Eq.(7)
  - 7:     **for**  $i=1:M$  (all particles) **do**
  - 8:         updating velocity  $V_i$  by Eq.(1)
  - 9:         updating particle position  $X_i$  by Eq.(2)
  - 10:         *Initializing BP* with new  $X_i$  and *calculating fitness* by Eq.(11)
  - 11:         **if**  $X_i$  is better than  $p_{id}$
  - 12:             Set  $X_i$  is to be  $p_{id}$
  - 13:         **End if**
  - 14:         **if**  $X_i$  is better than  $p_{gd}$
  - 15:             Set  $X_i$  is to be  $p_{gd}$
  - 16:         **End if**
  - 17:     **End for**  $i$
  - 18:      $iter = iter + 1$
  - 19: **End While**
  - 20: *Initializing BP* with  $p_{gd}$
  - 21: *Inputting and obtaining the predicted output*
- 

121 The formula for calculating the  $i$ -th particle fitness is defined as

$$f_i = \frac{1}{S} \sum_{s=1}^S \sum_{j=1}^m (Y_{sj} - \hat{Y}_{sj})^2 \quad (11)$$

where  $S$  is the number of training set samples,  $m$  is the output neurons number,  $Y_{sj}$  is the  $j$ -th true output of the  $s$ -th sample, and  $\hat{Y}_{sj}$  is the corresponding predict output.

### 3 Algorithm Testing

In order to investigate the COPSO-BP performance and reliability, Rosenbrock and Bohachevsky testing functions were adopted, which are typical non-convex functions and mainly to evaluate the performance of unconstrained algorithms. However, due to the random nature of the function, it is not easy to solve and has a global minimum function value of zero.

(1) *Rosenbrock* function:

$$f_1(x) = 100 \times (x_1^2 - x_2)^2 + (1 - x_1)^2, x_i \in [-10, 10], i = 1, 2 \quad (12)$$

(2) *Bohachevsky* function:

$$f_2(x) = x_1^2 + x_2^3 - x_1 x_2 x_3 + x_3 - \sin(x_2^2) - \cos(x_1 x_3^2), x_i \in [-2\pi, 2\pi], i = 1, 2, 3 \quad (13)$$

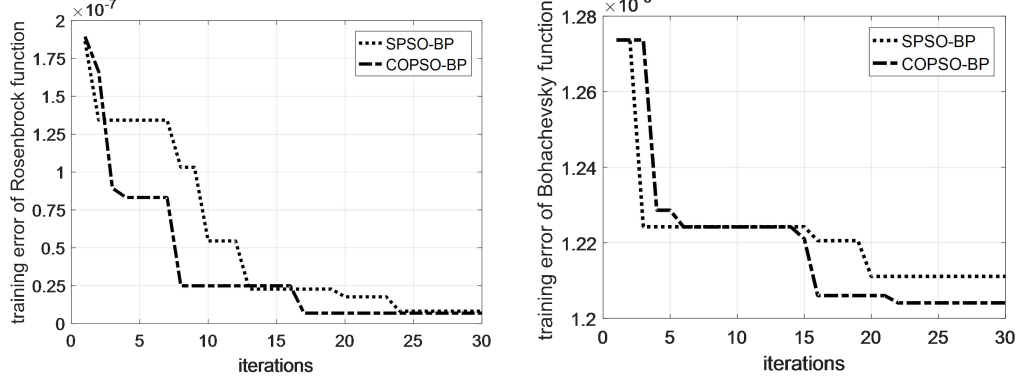
The standard PSO-BP (SPSO-BP) with linear decreasing inertia weight as Eq.(3), the COPSO-BP were carried out respectively. The three-layer BP of  $n$ - $s$ -1 structure is constructed with different hidden nodes. The PSO parameters are population size  $M = 60$ , learning factors  $c_1 = c_2 = 2.0$ , the maximum iteration  $T_{\max} = 30$ , inertia weight  $\omega_s = 0.9$ ,  $\omega_e = 0.4$ ,  $x_0 = 0.234$  and  $\mu = 4$  for chaotic parameters, the search dimension  $D = n \times s + s \times 1 + s + 1$  which includes all the neuron weights and thresholds. For BP network, 150 training samples and 50 testing samples were randomly produced within the variable range. The training error is defined as

$$E = \frac{1}{S} \sum_s (T_s - O_s)^2 \quad (14)$$

where  $S$  is the training samples number,  $T_s$ ,  $O_s$  are the expected and predicted output for training sample  $s$  respectively. The network structures with minimum training errors for *Rosenbrock* and *Bohachevsky* functions are 2-7-1 and 3-6-1 respectively. The simulation performs 20 times for each testing function with SPSO-BP and COPSO-BP algorithms. The numerical result was shown in Table.2. One of the evolutionary training error curves (select one in 20 times randomly) were shown in Fig.3, and the fitting curves of COPSO-BP algorithm were shown in Fig.4.

**Table.2** Comparison of SPSO-BP and COPSO-BP algorithm for testing functions

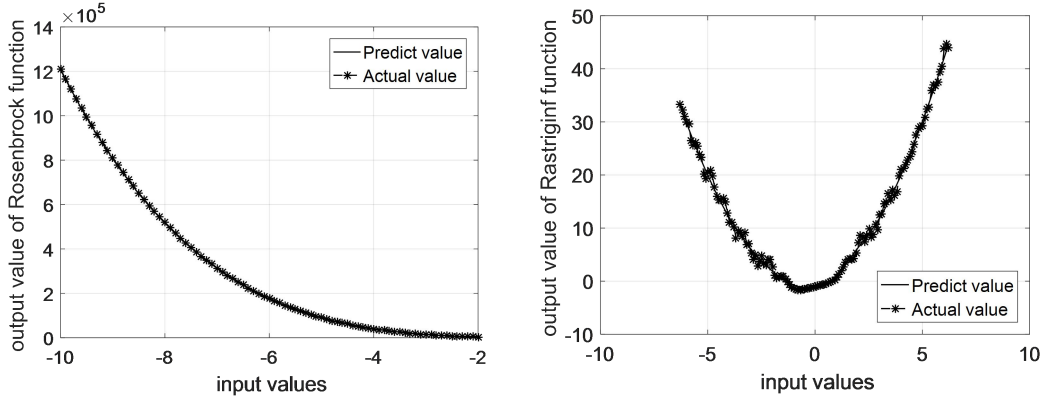
Testing functions	SPSO-BP		COPSO-BP	
	Average value	Optimal value	Average value	Optimal value
<i>Rosenbrock</i>	2.375e-3	2.300e-5	1.201e-3	2.410e-06
<i>Bohachevsky</i>	0.225	1.024e-3	0.193	3.360e-4



149

150

**Fig. 3** Training error curves of SPSO-BP and COPSO-BP algorithms



151

152

**Fig. 4** Fitting curves of COPSO-BP algorithm

153

154

155

156

157

It can be seen in Table.2 that both the SPSO-BP and COPSO-BP algorithms can acquire a relative high accuracy for testing functions, the COPSO-BP is a slightly better than SPSO-BP. However, the COPSO-BP has better convergence rate and optimization efficiency in the early stage in Fig.3. Therefore, the SPSO-BP and COPSO-BP algorithms have strong learning ability, good stability and generalization ability, which will be suitable for TEM inversion.

158

## 4 Layered model and parameter analysis

159

### 4.1 Forward Model

160

According to Kaufman's derivation (1983), the frequency response of central loop source for the layered model takes the following Hankel transform

162

$$H_z(\rho, \omega) = Ia \int_0^{\infty} \frac{m^2}{m + m_1/R_1^*} J_1(m\rho) dm \quad (15)$$

163

164

165

166

167

where  $a$  is the radius of transmitting coil,  $I$  is the excitation current,  $\rho$  is the center distance between the transmitting coil and the receiving coil,  $J_1(m\rho)$  is the first-order Bessel function,  $m$  is integral variable,  $m_1 = (m^2 - k_1^2)^{1/2}$ ,  $k_1$  is the conduction current,  $\sigma_1$  is the conductivity,  $k_1 = -i\omega\mu\sigma_1$ , and  $R_1^*$  is the first layer apparent resistivity conversion function which can be obtained by the following recurrence formula

168

$$\begin{cases} R_n^* = 1 \\ R_j^* = \frac{m_j R_{j+1}^* + m_{j+1} \text{th}(m_j h_j)}{m_{j+1} + m_j R_{j+1}^* \text{th}(m_j h_j)} \end{cases} \quad (16)$$

169 There is no analytical solution for the time-domain response for layered model, it can only be  
 170 solved by numerical calculation. The Hankel transform in formula (15) is calculated by an  
 171 improved digital filtering algorithm with 47 points  $J_1$  filter coefficient, and then time response can  
 172 be obtained using the Gaver-Stehfest transform as follows:

$$173 \quad H_z(\rho, t) = \frac{\ln 2}{t} \sum_{n=1}^N K_n H_z(\rho, s_n) \quad (17)$$

174 where  $s_n = (\ln 2/t) \times n$ ,  $K_n$  is the coefficient,  $N$  is determined by the computer bits, generally  $N=12$ .

175 The ramp excitation current of TEM is

$$176 \quad I(t) = \begin{cases} 0, & t < 0 \\ t/T_1, & 0 \leq t < T_1 \\ 1, & T_1 < t \end{cases} \quad (18)$$

177 where  $T_1$  is the turn-off time, and the Laplace transform is

$$178 \quad I(s) = \frac{1}{T_1 s^2} - \frac{1}{T_1 s^2} e^{-T_1 s} = \frac{1}{T_1 s^2} (1 - e^{-T_1 s}) \quad (19)$$

179 Therefore, for a specific layered model, the apparent resistivity conversion function  $R_1^*$  is firstly  
 180 calculated by recurrence formula (16) based on geoelectric structure parameters. And then the  
 181 frequency response at fixed point  $H_z(\omega)$  is calculated by Hankel transform as formula (15). For  
 182 ramp excitation, the Laplace transform of  $H_z(s)$  should multiplied by  $I(s)$ . Finally, the time  
 183 response  $H_z(t)$  is obtained by Gaver-Stehfest transform as formula (17). So the  $H_z(t)$  is obtained by  
 184 a Gaver-Stehfest transform, a Hankel transform and a recurrence calculation, and it is somewhat  
 185 heavy computational consuming.

186 However, the vertical magnetic field  $H_z(t)$  is the actual observed signal in transient  
 187 electromagnetic method in engineering applications. It is the inversion input and output is  
 188 geoelectric structure parameters. A method which can avoid the complicated forward model  
 189 calculation is of great importance in algorithm efficiency.

## 190 4.2 BP network design and COPSO algorithm

191 For BP structure, the output nodes are determined by the number of inversion geoelectrical  
 192 parameters, the input nodes are determined by the samples number of  $H_z(t)$ , the hidden nodes  
 193 varies according to approximation performance. As a three-layer or five-layer geoelectric model,  
 194 its geoelectrical parameters are 5 (three resistivity and two thickness parameters) or 9 (five  
 195 resistivity and four thickness parameters), the output nodes are 5 or 9 correspondingly. The  
 196 characteristic samplings of  $H_z(t)$  are chosen as 10 or 20, which are determined by the model's  
 197 complexity, more layers mean mores sampling points needed. The 10 samplings were selected in  
 198 this paper hence with 10 input nodes. While for the hidden layer neuron, its number is related to  
 199 the weights and threshold parameters amount directly and affects the BP performance greatly. An



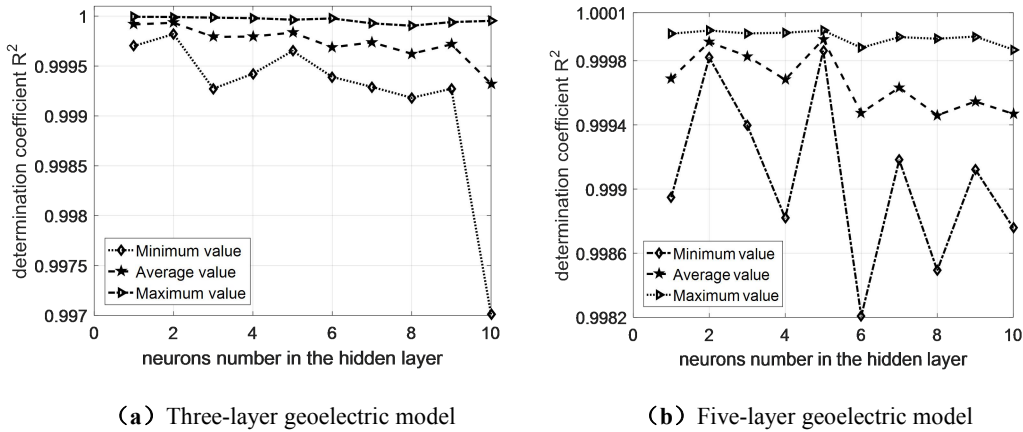
200  
201

appropriate hidden nodes number is necessary and a determination coefficient  $R^2$  is defined for evaluating as

$$R^2 = \frac{\left( n \sum_{i=1}^n Y_i \hat{Y}_i - \sum_{i=1}^n Y_i \sum_{i=1}^n \hat{Y}_i \right)^2}{\left( n \sum_{i=1}^n \hat{Y}_i^2 - \left( \sum_{i=1}^n \hat{Y}_i \right)^2 \right) \left( n \sum_{i=1}^n Y_i^2 - \left( \sum_{i=1}^n Y_i \right)^2 \right)} \quad (20)$$

203  
204  
205  
206  
207  
208  
209

where  $Y_i$  is the true value,  $\hat{Y}_i$  is the predicted value for  $i$ -th training data,  $n$  is the training data number. A larger determination coefficient means a better approximation performance. The simulations on hidden nodes effect were carried out for a three-layer and five-layer geoelectric models. The BP structure is 10- $s$ -5 and 10- $s$ -9, its transfer, training and learning functions are ‘Log sigmoidal’, ‘Levenberg-Marquardt’ and ‘Gradient descent momentum’ respectively. The average, minimum and maximum value of  $R^2$  were obtained after running 20 times for each simulation. The  $R^2$  curves were shown in Fig.5.



210  
211

**Fig. 5** Influence of hidden layer nodes on  $R^2$  for different geoelectric model

212  
213  
214  
215  
216

It can be seen that the optimal neural network structures were 10-2-5 and 10-5-9 for three and five-layer models based on the maximum  $R^2$ . Then, the PSO-BP algorithms with different inertia weight were implemented and compared for three-layer model. The BP structure was chosen as 10-2-5, four types of inertia weight as Eq. (3~7) in PSO were compared in Table.3.

217

**Table.3** Comparison of different inertia weights in PSO algorithms ( $\omega_s = 0.9$ ,  $\omega_e = 0.4$ )

inertia weight	iteration number	minimum fitness	average fitness	convergence time(s)
$\omega_1$	9	1.3914e-3	1.3982e-3	65.21
$\omega_2$	29	1.4406e-3	1.4418e-3	204.97
$\omega_3$	25	1.4168e-3	1.4224e-3	189.17
$\omega_c$	6	1.3846e-3	1.3925e-3	44.34

218  
219  
220

The simulation was implemented on Core (TM) i5-7500 with 8GB memory. It is obviously found in Table.3 that the COPSO algorithm has much faster convergence rate, less iteration number and time consuming.

221 **4.3 Layered model inversion**

222 A 3-layered and 5-layered geoelectric models were investigated, which the PSO parameter values  
 223 are the same as those of the Algorithm Testing parts in the paper. In order to simulate actual TEM  
 224 applications, the ramp turn-off is taken into account. Considering the probability distribution  
 225 characteristic of above algorithms, the average of 20 simulation results is chosen. The BP,  
 226 SPSO-BP, COPSO-BP algorithms and non-linear programming genetic algorithm (NPGA) (Li et  
 227 al., 2017) were compared.

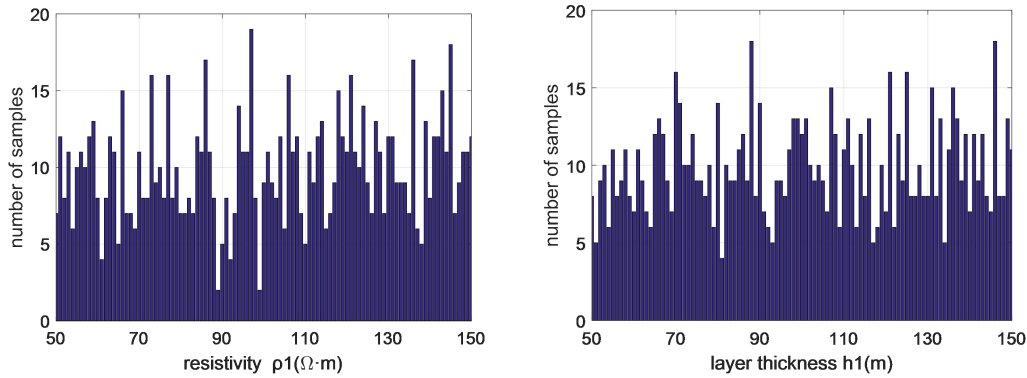
228 **(1) 3-layered H type model**

229 The central loop TEM parameters are set as following, transmitting coil radius  $a = 100$  m, ramp  
 230 emission current is 100 A, turn-off time is 1  $\mu$ s. In the geoelectric model, the resistivity  $\rho_1 = 100$   
 231  $\Omega \cdot m$ ,  $\rho_2 = 10 \Omega \cdot m$ ,  $\rho_3 = 100 \Omega \cdot m$  and thickness  $h_1 = 100$  m,  $h_2 = 200$  m.

232 The BP training samples which is a series of  $H_z(t)$  for different geoelectrical parameters were  
 233 generated by TEM forward model. The resistivity ranges were  $\rho_1 \in (50,150)$ ,  $\rho_2 \in (5,15)$ ,  
 234  $\rho_3 \in (50,150)$ , the thickness range were  $h_1 \in (50,150)$ ,  $h_2 \in (100,300)$ , and choosing 1000 random  
 235 groups. The resistivity and thickness distributions of  $\rho_1$  and  $h_1$  were shown in Fig.6. The relative  
 236 error is defined as

$$237 \quad Err_{rel} = \left| \frac{T_{cal}^* - O_{ref}^*}{O_{ref}^*} \right| \quad (21)$$

238 where  $T_{cal}^*$ ,  $O_{ref}^*$  are the calculated and reference value for the geoelectric models.



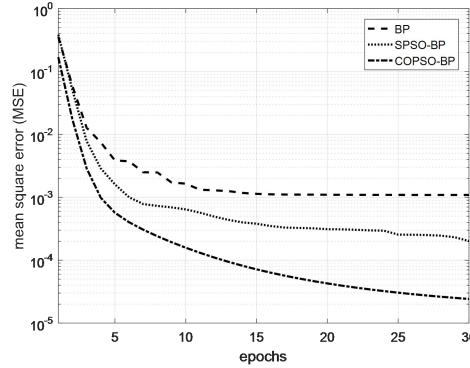
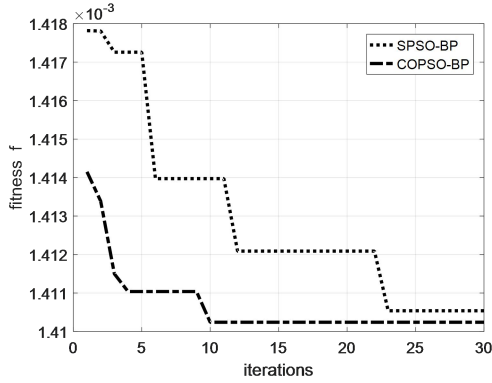
239  
 240 **Fig. 6** Distribution of resistivity  $\rho_1$  and thickness  $h_1$  in training samples

241 The inversion results were shown in Table.4. and Fig.7~8. The BP type algorithms were  
 242 superior to the NPGA inversion in Table.4. Moreover, the inversion accuracy, convergence rate  
 243 and optimization ability of the COPSO-BP algorithm were better than others.

244 **Table.4** Inversion comparison of three-layer H type geoelectric model

H type	resistivity $\rho$ ( $\Omega \cdot m$ )			thickness $h$ (m)		total relative error(%)
	$\rho_1$	$\rho_2$	$\rho_3$	$h_1$	$h_2$	

true values	100	10	100	100	200	--
BP relative error(%)	-0.275	-0.625	0.765	-0.968	-0.649	3.284
SPSO-BP relative error(%)	0.062	-0.322	-0.737	-0.579	-0.970	2.672
COPSO-BP	100.031	9.991	99.310	100.234	200.886	--
COPSO-BP relative error(%)	0.031	-0.087	-0.689	0.234	0.443	1.487
NPGA relative error(%)	0.133	-0.034	3.450	-7.305	-0.401	11.323



245 **Fig. 7** Fitness curves of SPSO-BP and COPSO-BP      **Fig. 8** Mean square error curves comparison

246 Additional results showed that the solution range of  $\rho_1$  and  $h_1$  in 20 times simulations for above  
247 algorithms were  $\rho_1 \in (97.980, 103.102)$ ,  $h_1 \in (96.962, 102.480)$  for BP,  $\rho_1 \in (98.954, 101.137)$ ,  
248  $h_1 \in (96.955, 101.829)$  for SPSO-BP,  $\rho_1 \in (99.382, 100.989)$ ,  $h_1 \in (97.877, 101.044)$  for COPSO-BP  
249 respectively. Therefore, the COPSO-BP can acquire higher accuracy and is more stable.

251 **(2) 5-layered KHK type model**

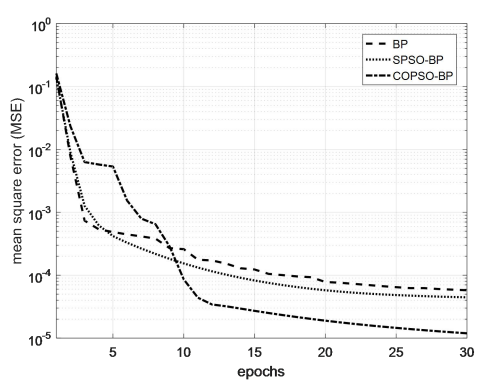
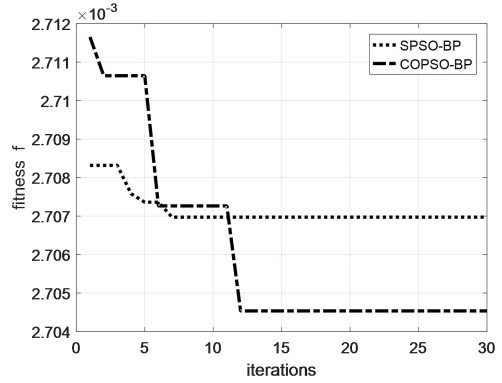
252 A 5-layered KHK type geoelectric model was adopted and its resistivity were  $\rho_1 = 100 \Omega \cdot m$ ,  $\rho_2 =$   
253  $300 \Omega \cdot m$ ,  $\rho_3 = 50 \Omega \cdot m$ ,  $\rho_4 = 200 \Omega \cdot m$ ,  $\rho_5 = 30 \Omega \cdot m$  and thickness were  $h_1 = 100 m$ ,  $h_2 = 200 m$ ,  $h_3$   
254  $= 300 m$ ,  $h_4 = 500 m$ .

255 The training samples with parameter ranges were  $\rho_1 \in (50, 150)$ ,  $\rho_2 \in (150, 450)$ ,  $\rho_3 \in (25, 75)$ ,  
256  $\rho_4 \in (100, 300)$ ,  $\rho_5 \in (15, 45)$  for resistivity, and  $h_1 \in (50, 150)$ ,  $h_2 \in (100, 300)$ ,  $h_3 \in (150, 450)$ ,  
257  $h_4 \in (250, 750)$  for thickness. The 1000 groups training samples were generated within above  
258 ranges. The inversion results were shown in Table.5 and Fig.9~10. As can be seen that the  
259 COPSO-BP algorithm has better global optimization performance.

260 **Table.5** Inversion comparison for five-layer KHK type geoelectric model

KHK type	resistivity $\rho(\Omega \cdot m)$					thickness $h(m)$				Total relative error(%)
	$\rho_1$	$\rho_2$	$\rho_3$	$\rho_4$	$\rho_5$	$h_1$	$h_2$	$h_3$	$h_4$	
true values	100	300	50	200	30	100	200	300	500	--
BP relative error(%)	-1.006	-0.862	-1.014	-0.030	1.119	-0.362	-0.298	-0.575	-0.376	5.645
SPSO-BP relative error(%)	0.429	1.040	-0.577	-0.071	-0.883	-0.002	0.657	-0.655	-0.316	4.634

COPSO-BP	99.594	299.469	50.082	199.092	29.937	99.501	200.481	301.800	497.670	--
COPSO-BP relative error(%)	-0.405	-0.176	0.164	-0.453	-0.209	-0.498	0.240	0.600	-0.465	3.214
NPGA relative error(%)	-6.211	-0.008	-0.974	3.930	3.083	-0.691	0.505	-2.900	-3.370	19.062



261

262 **Fig. 9** Fitness curves of SPSO-BP and COPSO-BP

**Fig. 10** Mean square error curves comparison

263 **(3) Inversion comparison**

264 Three kinds of BP methods as traditional BP, the SPSO-BP and the COPSO-BP algorithms were  
 265 compared in Table.6. Hence, the training times of COPSO-BP was obviously less than SPSO-BP  
 266 and was almost equal to BP, it can obtain better precision especially for its global optimization  
 267 performance.

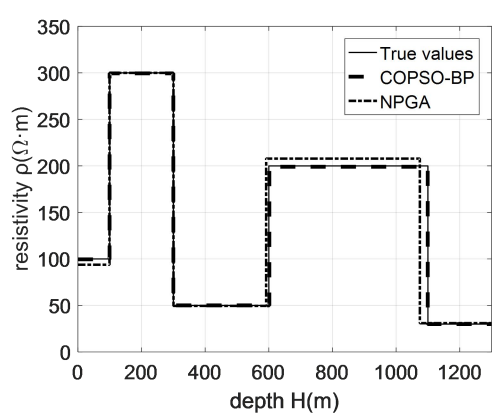
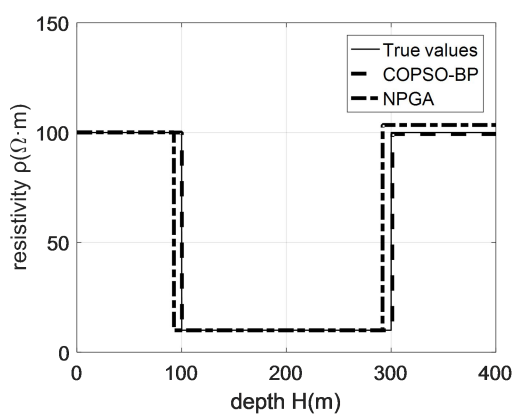
268 **Table.6** Simulation comparison for different algorithms

inversion method	three-layer H type model			five-layer KHK type model		
	training times	minimum training error	test relative error rate(%)	training times	minimum training error	test relative error rate(%)
BP	3	0.2882	3.284	5	0.3013	5.645
SPSO-BP	7	0.2832	2.672	15	0.2992	4.634
COPSO-BP	5	0.2725	1.487	6	0.2900	3.214

269

270

The inversion of COPSO-BP and NPGA were compared in Fig.11. The fitting ability of COPSO-BP was much better than NPGA.



271

272 (a) Three-layer H type geoelectric model (b) Five-layer KHK type geoelectric model

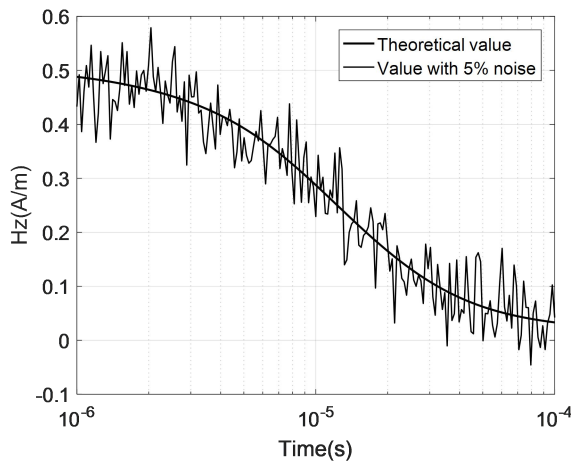
273 Fig. 11 Inversion comparison for different geoelectric models

274 (4) Robust performance analysis

275 In order to verify the algorithm robustness, 5%(26dB) and 10%(20dB) Gaussian random noise  
 276 was added in TEM data for three-layer geoelectric model. Three kinds of inversions were  
 277 implemented respectively. The results and comparison were shown in Table.7. The  $H_z(t)$  and data  
 278 with 5% noise were shown in Fig.12.

279 Table 7 Comparison of inversion results for three-layer H type (with noise) model

model parameters	resistivity $\rho(\Omega \cdot m)$			thickness h(m)		Total relative error(%)	
	$\rho_1$	$\rho_2$	$\rho_3$	$h_1$	$h_2$		
true value	100	10	100	100	200	--	
without noise	BP	99.724	9.937	100.765	99.031	198.701	3.284
	COPSO-BP	100.031	9.991	99.310	100.234	200.886	1.487
5% noise	BP	101.374	9.966	98.283	101.255	199.282	5.039
	COPSO-BP	100.252	9.977	98.222	101.206	199.228	3.847
10% noise	BP	90.525	9.931	99.481	101.748	203.105	13.976
	COPSO-BP	104.472	9.96050	101.345	100.570	199.437	7.064



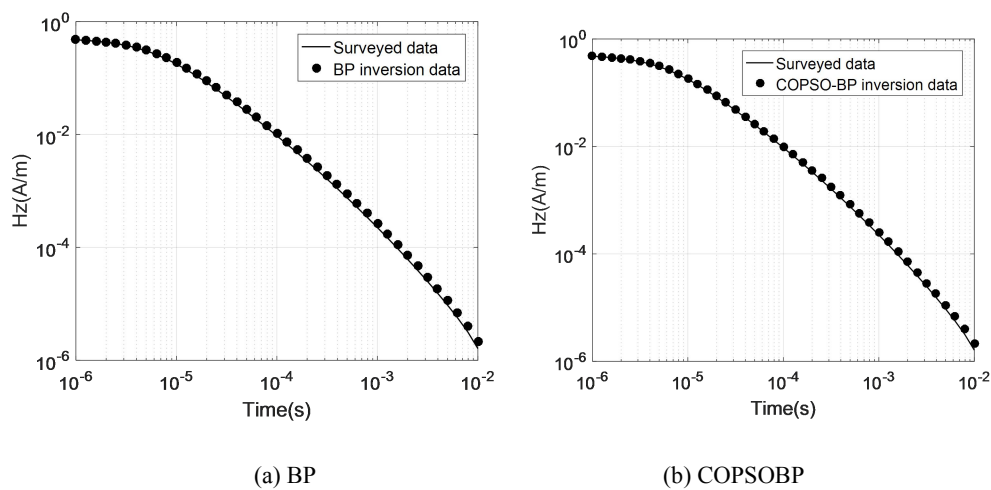
280  
 281 Fig.12 Forward data of  $H_z$  and data with 5% noise

282 As can be seen from Table 3, after applying 5% and 10% Gaussian noise the COPSO-BP  
 283 inversion has higher robust ability. The accuracy was obviously improved based on the total  
 284 relative error data.

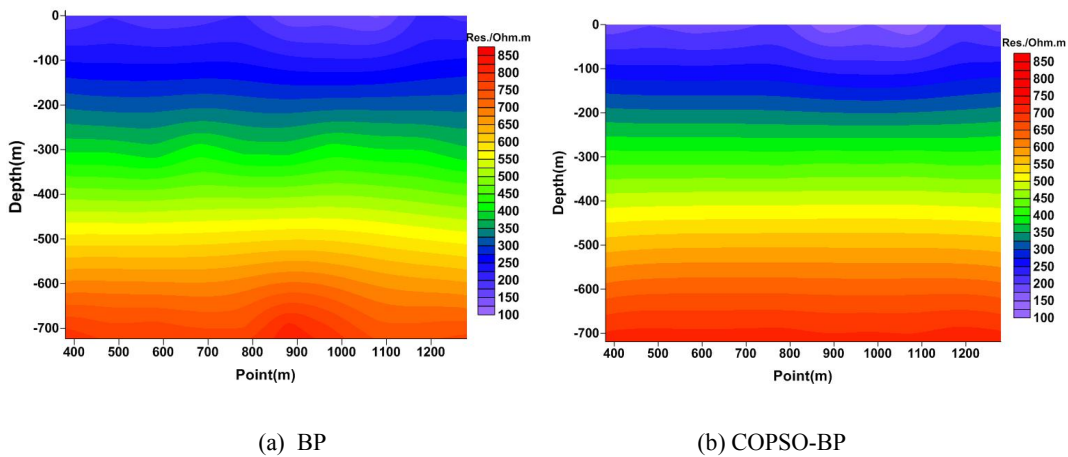
285 4.4 Field example

286 In order to test the effectiveness of the method, a transient electromagnetic vertical magnetic field  
 287 ( $H_z$ ) with 10 measuring points at the 380m to 1280m of the No. 1 line from a mining area in  
 288 Anhui Province was selected. After the data processing, the inversion was performed using the

289 3-layer neural network model in the previous section, and the results of BP and COPSOBP  
 290 inversion were compared. Figure 13 shows the comparison between the surveyed data and the  
 291 inversion data at 380m of the No. 2 line in the mining area. Figure 14 displays the pseudo-sections  
 292 of the 10 sets of inversion data combined with the geological data interpolation smoothing. It can  
 293 be seen from Fig. 14 that the first layer is a low resistivity (100~200  $\Omega\cdot m$ ), which is inferred to be  
 294 the second layer (T2g22) gray dolomite of the Middle Triassic old Malague section, with a  
 295 thickness of about 200 m; the second layer is the second highest resistivity (300~400  $\Omega\cdot m$ ), which  
 296 is surmised to be the first layer (T2g21) dolomite of the Middle Triassic old Malaga section, with a  
 297 thickness of about 400m; the third layer is high resistivity (600~800 $\Omega\cdot m$ ), which is speculated to  
 298 be the 6th layer (T2g16) limestone dolomite of the Middle Triassic old group. The results are  
 299 basically consistent with the geological conditions of the mining area, indicating the feasibility  
 300 and effectiveness of the neural network method. And the results of COPSO-BP inversion are better  
 301 than those of BP, which the inversion position is more accurate, the shape and spacing are clearer,  
 302 and the resistivity of each layer is more consistent with the those of the actual geological model.



303  
304  
305 **Figure 13.** 1D inversion forward results. (a) BP; (b) COPSOBP.



306  
307  
308 **Figure 14.** Inversion results of BP (a) and COPSO-BP (b).

309 **5 Discussion**

310 The inversion is performed for 3-layered (H-type) and 5-layered (KHK-type) geoelectric models  
311 in this paper. The results show that the BP neural network is better than the NPGA algorithm,  
312 because the BP method does not need to use the forward algorithm repeatedly, and its calculation  
313 time is short, which is different from the nonlinear heuristic method based on global space search  
314 solution.

315 The BP main advantage is that it can interpret the transient electromagnetic sounding results  
316 quickly after training the network. Furthermore, BP algorithm could automatically obtain the  
317 "reasonable rules" between input and output data by learning, and it can adaptively store the  
318 learning content in the network weight, which the BP neural network has the high self-learning  
319 and self-adaptation ability. In addition, the superior simulation results of the test function indicate  
320 that the BP algorithm can approximate any nonlinear continuous function with arbitrary precision,  
321 which means it has strong nonlinear mapping ability; the inversion results of the layered  
322 geoelectric model with uncorrelated noise data prove that the BP algorithm has strong robustness,  
323 which means it has the ability to apply learning results to new knowledge. However, the BP neural  
324 network weight is gradually adjusted by the direction of local improvement, which causes the  
325 algorithm to fall into local extremum, and the weight converges to a local minimum that leads to  
326 the network training failure; Moreover, BP is very sensitive to the initial network weight, and the  
327 initialization network with different weight values tends to converge to different local minimums,  
328 so that obtains different results each time; In addition, the BP algorithm is a gradient descent  
329 method essentially, which leads to a slow convergence rate.

330 From the results of the layered model and parametric analysis part, it can be seen that single  
331 BP algorithm has higher error value than SPSO-BP, because BP method is sensitive to initial  
332 weight and easy to fall into local minimum values, thus a heuristic global search particle swarm  
333 optimization algorithm with simple structure, rapid convergence and high precision is applied to  
334 optimize the weight and threshold of BP neural network, which improves the global optimization  
335 performance of the algorithm. Furthermore, the PSO algorithm adjusts the inertia weight  
336 adaptively based on the chaotic oscillation curve that is similar to the annealing process in the  
337 simulated annealing algorithm (SA), which jumps out the local extremum faster in the early stage  
338 and accelerates the convergence and reduces the training times. Therefore, compared with  
339 SPSO-BP and BP algorithm, the inversion results of COPSO-BP are closer to the theoretical data  
340 with smaller error fluctuations, stronger anti-noise, better generalization performance and higher  
341 stability, which it is effective in solving geophysical inverse problems.

342 From the simulation experiment, it is not clear how the weight organization affects the BP  
343 neural network weight learning process. It is necessary to conduct a more systematic study on this  
344 problem to improve our understanding of how BP neural network handles training data.

## 345 **6 Conclusion**

346 The nonlinear COPSO-BP method was proposed for TEM inversion. The BP's initial weight and  
347 threshold parameters were trained by COPSO algorithm which makes it not easy to fall into local  
348 optimum. The chaotic oscillation inertia weight for PSO was proposed so as to improve the PSO's  
349 global optimization ability and fast convergence in early stage. The layered geoelectric model  
350 inversion showed that the COPSO-BP method has better accuracy, stability and relative less  
351 training times.

## 353 **Author Contributions**

354 Huaqing Zhang conceived this manuscript. Huaqing Zhang and Ruiyou Li developed the main  
355 algorithmic idea and mathematical part. Ruiheng Li and Nian Yu carried out the simulation and  
356 data analysis. Qiong Zhuang completed the writing and interpretation of this manuscript. All  
357 authors contributed to the manuscript writing and approved the final manuscript.

## 359 **Competing interests**

360 The authors declare that they have no conflict of interest.

## 362 **Acknowledgments**

363 This work was partly supported by the National Natural Science Foundation of China  
364 (No.51377174, No.51577016, No.51877014), the Fundamental Research Funds for the Central  
365 Universities(No.2018CDQYDQ0005).

## 366 **Computer Code Availability**

367 Code name is PSOBP, developer is Huaqing Zhang and Ruiyou Li, contact address is  
368 Chongqing University in China, telephone number is 13752954568 and e-mail is  
369 zhanghuaqing@cqu.edu.cn, year first available, hardware required is a computer, software  
370 required is MATLAB R2016a, program language is C++, program size is 10KB, and source code  
371 from <https://github.com/liruiyou/PSOBP>.

## 372 **Reference**

- 373 Dai, Q., Jiang, F., and Dong, L.: Nonlinear inversion for electrical resistivity tomography based on chaotic DE-BP  
374 algorithm, *J. Cent. South. Univ.*, 21, 2018-2025, <https://doi.org/10.1007/s11771-014-2151-9>, 2014.
- 375 Fernández Martínez, J. L., García Gonzalo, E., Fernández Álvarez, J. P., Kuzma, H. A., and Menéndez Pérez, C. O.:  
376 PSO: A powerful algorithm to solve geophysical inverse problems: Application to a 1D-DC resistivity case,  
377 *Journal of Applied Geophysics*, 71, 13-25, <https://doi.org/10.1016/j.jappgeo.2010.02.001>, 2010.
- 378 Godio, A., and Santilano, A.: On the optimization of electromagnetic geophysical data: Application of the PSO  
379 algorithm, *Journal of Applied Geophysics*, 148, 163-174, <https://doi.org/10.1016/j.jappgeo.2017.11.016>, 2018.



380 Wang, H., Liu M. L., Xi, Z. Z., Peng, X. L., He, H.: Magnetotelluric inversion based on BP neural network  
381 optimized by genetic algorithm, *Chinese Journal of Geophysics*, 61, 1563-1575 <https://doi.org/10.6038/cjg>  
382 2018L0064, 2018.

383 Jha, M. K., Kumar, S., and Chowdhury, A.: Vertical electrical sounding survey and resistivity inversion using  
384 genetic algorithm optimization technique, *J. Hydrol.*, 359, 71-87, <https://doi.org/10.1016/j.jhydrol.2008.06.018>,  
385 2008.

386 Jiang, F., Dai, Q., and Dong, L.: An ICPSO-RBFNN nonlinear inversion for electrical resistivity imaging, *J. Cent.*  
387 *South. Univ.*, 23, 2129-2138, <https://doi.org/10.1007/s11771-016-3269-8>, 2016a.

388 Jiang, F., Dai, Q., and Dong, L.: Nonlinear inversion of electrical resistivity imaging using pruning Bayesian  
389 neural networks, *Journal of Applied Geophysics*, 13, 267-278, <https://doi.org/10.1007/s11770-016-0561-1>,  
390 2016b.

391 Jiang, F., Dong, L., and Dai, Q.: Electrical resistivity imaging inversion: An ISFLA trained kernel principal  
392 component wavelet neural network approach, *Neural. Networks.*, 104, 114-123, <https://doi.org/10.1016/j.neunet>.  
393 2018.04.012, 2018.

394 Kaufman, A. A., and Keller, G. V.: *Frequency and Transient Sounding*, Elsevier Methods in Geochemistry &  
395 Geophysics, 1983.

396 Johnson, O. L., Aizebeokhai, A. P.: Application of Artificial Neural Network for the Inversion of Electrical  
397 Resistivity Data, *Journal of Informatics and Mathematical Sciences*, 9, 297-316, 2017.

398 Li, F. P., Yang, H. Y., and Liu, X. H.: Nonlinear programming genetic algorithm in transient electromagnetic  
399 inversion, *Geophysical and Geochemical Exploration*, 41, 347-353, 2017.

400 Maiti, S., Erram, V. C., Gupta, G., and Tiwari, R. K.: ANN based inversion of DC resistivity data for groundwater  
401 exploration in hard rock terrain of western Maharashtra (India), *J. Hydrol.*, 464, 294-308,  
402 <https://doi.org/10.1016/j.jhydrol.2012.07.020>, 2012.

403 Pekşen, E., Yas, T., and Kıyık, A.: 1-D DC Resistivity Modeling and Interpretation in Anisotropic Media Using  
404 Particle Swarm Optimization, *Pure. Appl. Geophys.*, 171, 2371-2389,  
405 <https://doi.org/10.1007/s00024-014-0802-2>, 2014.

406 Raj, A. S., Srinivas, Y. , and Oliver, D. H.: A novel and generalized approach in the inversion of geoelectrical  
407 resistivity data using Artificial Neural Networks (ANN), *J. Earth Syst. Sci.*, 123, 395-411,  
408 <https://doi.org/10.1007/s12040-014-0402-7>, 2014.

409 Rosas-Carbajal, M., Linde, N., Kalscheuer, T., and Vrugt, J. A.: Two-dimensional probabilistic inversion of  
410 plane-wave electromagnetic data: methodology, model constraints and joint inversion with electrical resistivity  
411 data, *Geophys. J. Int.*, 196, 1508-1524, <https://doi.org/10.1093/gji/ggt482>, 2014.

412 Shi, F., Wang, X. C., and YUN L.: *Matlab neural network case study*, The Beijing University of Aeronautics &  
413 Astronautics Press, Beijing, 2010.

414 Sharma, S. P.: VFSARES—a very fast simulated annealing FORTRAN program for interpretation of 1-D DC  
415 resistivity sounding data from various electrode arrays, *Comput. Geosci.*, 42, 177-188,  
416 <https://doi.org/10.1016/j.cageo.2011.08.029>, 2012.

417 Shi, X. M., Xiao, M., Fan, J. K., Yang, G. S., and Zhang, X. H.: The damped PSO algorithm and its application for  
418 magnetotelluric sounding data inversion, Chinese Journal of Geophysics., 52, 1114–1120,  
419 <https://doi.org/10.3969/j.issn.0001-5733.2009.04.029>, 2009.

420 Srinivas, Y., Raj, A. S., Oliver, D. H., Muthuraj, D., and Chandrasekar, N.: A robust behavior of Feed Forward  
421 Back propagation algorithm of Artificial Neural Networks in the application of vertical electrical sounding data  
422 inversion, Geosci. Front., 3, 729-736, <https://doi.org/10.1016/j.gsf.2012.02.003>, 2012.

423 Tran, K. T., and Hiltunen, D. R.: Two-Dimensional Inversion of Full Waveforms Using Simulated Annealing, J.  
424 Geotech. Geoenviron. Eng., 138, <https://doi.org/1075-1090>, 2012.

425 Li, Y. Y., Chen, B. C., Zhao, Y. G., Yun, C., Ma, X. B., and Kong, X. R.: Nonlinear inversion for electrical  
426 resistivity tomography, Chinese Journal of Geophysics, 52, 758-764,  
427 [https://doi.org/10.1016/S1003-6326\(09\)60084-4](https://doi.org/10.1016/S1003-6326(09)60084-4), 2009.

428 Zhang, L. Y., and Liu, H. F.: The application of ABP method in high-density resistivity method inversion, Chinese  
429 Journal of Geophysics., 54, 64-71, <https://doi.org/10.1002/cjg2.1587>, 2011.